Received: 12 July 2022 | Revised: 13 October 2022 | Accepted: 26 October 2022

DOI: 10.1002/suco.202200624

ARTICLE

fib CEB-FIP WILEY

Experimental investigation of GFRP-reinforced concrete columns made with waste aggregates under concentric and eccentric loads

Arash Karimi Pour[1] | **Amir Shirkhani**[2] | **Mehmet Serkan Kırgız**[3] | **Ehsan Noroozinejad Farsangi**[4]

[1]Department of Civil Engineering, University of Texas at El Paso (UTEP), El Paso, Texas, USA

[2]Department of Structural Engineering, Faculty of Civil Engineering, University of Tabriz, Tabriz, Iran

[3]Department of Architecture, Faculty of Engineering and Natural Sciences, İstanbul Sabahattin Zaim University, İstanbul, Turkey

[4]Department of Civil Engineering, The University of British Columbia (UBC), Vancouver, Canada

Correspondence
Ehsan Noroozinejad Farsangi, Department of Civil Engineering, The University of British Columbia (UBC), Vancouver, Canada.
Email: ehsan.noroozinejad@ubc.ca

Abstract

Nowadays, reducing the waste and recycled material resources in nature and environmental protection, as well as reducing the use of natural resources, has gained the attention of engineers and researchers. One of the ways to reach this goal is to use waste and recycled materials in new concrete members' construction. Additionally, using glass fiber-reinforced polymer (GFRP) rebars has gained high consideration owing to their advantages such as high tensile strength and corrosion resistance. Therefore, this study aims to measure the influence of recycled coarse aggregates (RCA) on the structural performance of reinforced concrete (RC) columns reinforced by GFRP rebars under concentric and eccentric loading conditions. A total of 24 RC columns were cast and subjected to concentric and eccentric loads with different eccentricity ratios (e/h):0 (no eccentricity), 0.25 (moderate eccentricity), and e/h = 0.5 (high eccentricity). A total of 18 columns were strengthened with longitudinal GFRP rebars, and six specimens were considered control samples reinforced by steel rebars. RCA was used at two contents of 0% and 100% in terms of weight as a substitute for natural coarse aggregates (NCA). In addition, to measure the influence of transverse reinforcement, three different spacings were considered: 60, 120, and 180 mm. Evaluation of axial behavior, the strain of rebars and concrete, and the ductility were the main aims of this study. Moreover, a comparison between the experimental results and existing standards was carried out. Findings revealed the adequate axial resistance of specimens when RCA was used. Therefore, RCA incorporation improved the axial resistance of GFRP-RC columns by about 25% and 35% when the stirrup spacing declined by 60 and 120 mm, respectively in comparison with the same specimens made with NCA. However, the influence of RCA on the RC columns' axial behavior was declined by raising the eccentricity distance.

Discussion on this paper must be submitted within two months of the print publication. The discussion will then be published in print, along with the authors' closure, if any, approximately nine months after the print publication.

KEYWORDS

ductility, eccentric loading, GFRP-reinforced columns, RC column, recycled coarse aggregates

1 | INTRODUCTION

Due to some properties of glass fiber-reinforced polymer (GFRP) rebars such as corrosion strength, high tensile resistance, and electromagnetic transparency, interest in employing them as a substitute for steel rebars in reinforced concrete (RC) elements has grown. GFRP-reinforced RC columns have been given special attention among structural members as one of the main elements of concrete structures.[1–4] Many studies have been done to demonstrate the effect of using GFRP compared with steel on the axial behavior of RC columns.[5–11] De Luca and Nanni[12] presented a comprehensive overview of the behavior of concrete reinforced by GFRP bars. A discussion of design approaches for RC structures with internal GFRP bars follows the introduction of the mechanical and durability properties of both concrete and GFRP bars. They were also provided guidelines for the design of GFRP-RC structures, along with an overview of available test methods for the mechanical and durability characterization of both concrete and GFRP bars. The effect of the GFRP rebars ratio on the axial–flexural interaction behavior of RC columns was assessed by Guérin et al.[13] According to their study, the GFRP-RC columns exhibited larger tensile strains than the conventional concrete columns reinforced by steel rebars due to the high strength of GFRP. In another investigation, Hadhood et al.[14] evaluated the design requirements for GFRP-reinforced concrete columns. Findings showed numerous earlier proposed models to predict the operative bending stiffness. For GFRP-RC columns, the experimental-to-design capacity proportion ranged from 1.4 to 2.0. In addition to the properties of materials, the loading conditions play a crucial role to measure the axial performance of RC columns. For this aim, Abdelazim et al.[15] measured the influence of various test conditions on the performance of GFRP-RC slender columns under eccentric loads. The GFRP bars demonstrated their ability to maintain the stability and strength of RC columns under the effect of axial load. Also, to avoid stability failure, the permissible tensile designing strain of GFRPs was estimated to be restricted to 0.9. Under eccentric loading condition, Khorramian and Sadeghian[16] investigated the behavior of GFRP-RC short and slender rectangular concrete columns. They showed that after the concrete spalling, the columns were able to withstand the load, bending, and deformation up to the failure of GFRP reinforcement under axial stress. In another study, Chellapandian et al.[17] measured the effect of eccentric loadings on the structural responses of short RC column. They revealed that the strengthened RC column elements had significantly improved stiffness and strength, particularly when compressed eccentrically.

On the other hand, cement and aggregates are the most common parts of concrete mixture design; however, using cement and natural aggregates comes at a high cost and has negative environmental consequences (eg., carbon dioxide emissions that harm the environment and animals' lives as a result of cement production from factories). Therefore, recycled coarse aggregates (RCA) and other waste materials aid in conserving natural resources and can be utilized to make concrete elements as a substitute for cement or natural coarse aggregates (NCA). In this regard, the structural performance of concrete members made from various recycled materials has been studied in a variety of ways.[18–23] Breccolotti and Materazzi[24] investigated the eccentrically loaded performance of RCA-RC columns experimentally and numerically. Also, the effect of concrete compressive strength on the performance of RCA concrete was measured experimentally, and it revealed that RCA had a larger scattering in the compressive resistance. In another investigation, Choi and Yun[25] studied the uniaxial behavior of RCA-RC columns. Evaluation of the columns' failure mode, compressive resistance, and deformability were the main aims of their study. Besides, the ultimate compression resistance was compared with existing ACI 318-08 requirements. When the testing findings were compared with the ACI requirements, it was found that RCA columns meet the ACI specifications for axial load-bearing resistance. Xu et al.[26] measured the axial performance of RCA-RC columns. As per their findings, a bilinear technique was generated to predict the axial behavior of RC columns produced by RCA. They showed that the water absorption value of RCA significantly affected the compression behavior of RC columns, and the capacity of columns decreased by increasing the RCA contents due to their higher water absorption. Sunayana and Barai[27] studied the uniaxial behavior of RC columns produced by fly ash and RCA experimentally and numerically. The resistance of RCA-RC columns was around 9% greater than NCA columns. Tang et al.[28] assessed the axial performance of RCA concrete-filled GFRP–steel composite tube columns. Their findings demonstrated that using a GFRP tube

enhanced the axial load–displacement performance of RC columns produced by RCA. Moreover, using high RCA substitution contents with a high slenderness rate led to ductile failure.

According to the literature, RCA made from crushed stone, and demolished structures can be a viable and environmentally beneficial substitute for conservative aggregates for structural applications. Previous studies reported that the axial performance of RC columns reduces as a result of RCA incorporation.[29,30] while based on the authors' knowledge, there is no study to address the influence of RCA on the performance of RC columns subjected to concentric and eccentric Loads. Conversely, using GFRP rebars has shown superior performance compared with steel rebars in terms of the axial performance of RC columns. Therefore, in this study, the GFRP rebars were used as longitudinal reinforcement to mitigate the negative effect of RCA on the axial performance of RC columns. In addition, the influence of stirrup spacing and loading conditions were considered two important variables affecting the load-bearing capacity and deformation of concrete columns. Also, a comparison between the experimental results and existing standards was carried out, and a modification factor was recommended to predict the behavior of GFRP-RC columns made with RCA.

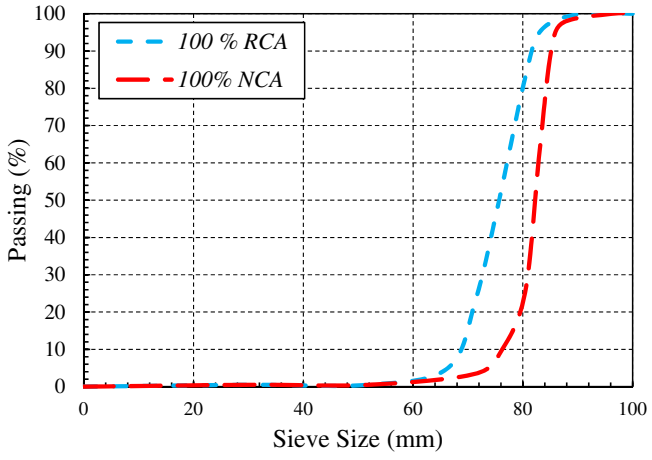

FIGURE 1 Used aggregates grading distribution. NCA, natural coarse aggregates; RCA, recycled coarse aggregates

2 | MATERIAL PROPERTIES AND SPECIMENS' CHARACTERISTICS

NCA and RCA were employed in this investigation. RCA was acquired via building destruction and used to replace NCA at two different weight fractions: 0% and 100%. The grading curves of aggregates are illustrated in Figure 1. Also, Table 1 shows the physical features of aggregates. Table 2 provides the concrete mix design. The entire water/cement fraction of all mixtures was kept constant at 0.4. Also, the chemical characteristics of used cement in this study are provided in Table 3, based on manufacturer information. Six 150 × 300 mm samples were manufactured and tested to determine the compressive and tensile strengths of concrete mixtures. The average

TABLE 2 Concrete mixes composition (kg/m^3)

Specimens	RCA	NCA	NFA	Cement
0SF-0RA	0	1320	1400	485
0SF-100RA	1320	0	1400	485

Abbreviations: NCA, natural coarse aggregates; NFA, natural fine aggregates; RCA, recycled coarse aggregates.

TABLE 3 Chemical components of used cement in this study

Component	Ordinary Portland cement composition (%)
CaO	64.64
SiO_2	21.28
Al_2O_3	5.60
Fe_2O_3	3.36
MgO	2.06
SO_3	2.14
N_2O	0.05
C3S	52.82
C2S	21.45
C3A	9.16
C4AF	10.2
Loss of ignition	0.64
Lime saturation factor	0.92

TABLE 1 Aggregate physical qualities

Type	Apparent density (g/cm^3)	Bulk density (g/cm^3)	Water absorption (wt%)	Crushing index (%)	Porosity (%)
NCA	2.58	2.72	1.508	33.1	3.57
RCA	2.47	2.63	1.224	47.5	2.74

Abbreviations: NCA, natural coarse aggregates; RCA, recycled coarse aggregates.

TABLE 4 Compressive and tensile strength of the various mixes

Group	Specimen	Average compressive resistance (MPa)	Compressive resistance coefficient of variation	Average tensile resistance (MPa)	Tensile resistance coefficient of variation
A	N-G-60-0	35.0	0.94	4.04	0.17
	N-G-60-50	37.3	1.54	4.03	0.15
	N-G-60-100	36.0	1.12	4.63	0.19
	R-G-60-0	39.3	1.63	3.78	0.10
	R-G-60-50	40.5	1.69	4.65	0.11
	R-G-60-100	40.0	0.81	4.05	0.11
B	N-G-120-0	36.5	1.78	3.84	0.15
	N-G-120-50	35.0	2.12	4.12	0.29
	N-G-120-100	35.0	1.65	3.24	0.21
	R-G-120-0	38.5	1.05	4.65	0.14
	R-G-120-50	39.0	1.85	5.25	0.28
	R-G-120-100	39.0	0.65	4.95	0.15
C	N-G-180-0	35.8	0.15	3.52	0.13
	N-G-180-50	36.2	0.18	4.04	0.11
	N-G-180-100	36.0	0.12	3.82	0.18
	R-G-180-0	37.8	1.68	4.65	0.35
	R-G-180-50	39.6	2.54	4.85	0.21
	R-G-180-100	39.0	0.56	4.65	0.32
D	N-S-180-0	36.0	1.35	3.56	0.25
	N-S-180-50	36.0	1.24	3.25	0.15
	N-S-180-100	35.6	1.18	3.70	0.28
	R-S-180-0	40.0	1.20	5.02	0.42
	R-S-180-50	40.0	2.12	4.85	0.14
	R-S-180-100	39.0	1.65	4.80	0.26

Note: N indicates specimens produced by 100% NCA; R indicates specimens produced by 100% RCA; G indicates the GFRP longitudinal rebars; S indicates the steel longitudinal rebars; The first and second numbers denote the stirrup spacing and eccentricity distance, respectively.
Abbreviations: GFRP, glass fiber-reinforced polymer; NCA, natural coarse aggregates; RCA, recycled coarse aggregates.

compressive and tensile resistances of three samples were utilized in each mix, as reported in Table 4.[31–34]

Furthermore, 22 mm diameter steel and GFRP rebars were used as longitudinal reinforcement. In addition, steel rebars with a 10 mm diameter were employed as a stirrup. Rebars were exposed to direct tension setup, and their characteristics were recorded as per ASTM D7957/D7957M[35] and ASTM A615/A615M[36] for steel and GFRP rebars, respectively. Their results are presented in Tables 5 and 6.

A total of 24 200 × 200 × 1000 mm short RC columns were cast and classified into four groups based on the category of rebars and stirrup spacing. All samples were longitudinally strengthened with four 22 mm GFRP reinforcements, resulting in a 3.79% rebars ratio. Table 7 provides the test matrix for four groups of samples: Groups A, B, and C's GFRP-reinforced columns had 60, 120, and 180 mm stirrup spacing, respectively, whereas group D's columns had longitudinal steel rebars with 60, 120, and 180 mm stirrup spacing. Group D specimens with 180 mm stirrup spacing were used as controllers, with maximum spacing equal to the smallest column dimension, 16 times the longitudinal bar diameter, or 48 times the tie diameter. Figure 2 shows the

TABLE 5 Rebars test results (GFRP)

	GFRP		
Diameter (mm)	Ultimate resistance (MPa)	Final strain (%)	Elastic moduli (GPa)
22	966	1.90	39.5

Abbreviation: GFRP, glass fiber-reinforced polymer.

TABLE 6 Rebars test results (steel)

	Steel				
Diameter (mm)	Yield strength (MPa)	Ultimate strength (MPa)	Yield strain (%)	Ultimate strain (%)	Modulus of elasticity (GPa)
10	371	561	0.13	0.25	210.10
22	408	677	0.15	0.26	218.17

TABLE 7 Properties of specimens

				Transverse reinforcement			
Group	Specimen	Aggregate type	f'_c (MPa)	Type	Spacing (mm)	Eccentricity (mm)	e/h (%)
A	N-G-60-0	NCA	32.2	GFRP	60	0	0
	N-G-60-50	NCA	32.2	GFRP	60	50	25
	N-G-60-100	NCA	32.2	GFRP	60	100	50
	R-G-60-0	RCA	34.5	GFRP	60	0	0
	R-G-60-50	RCA	34.5	GFRP	60	50	25
	R-G-60-100	RCA	34.5	GFRP	60	100	50
B	N-G-120-0	NCA	32.2	GFRP	120	0	0
	N-G-120-50	NCA	32.2	GFRP	120	50	25
	N-G-120-100	NCA	32.2	GFRP	120	100	50
	R-G-120-0	RCA	34.5	GFRP	120	0	0
	R-G-120-50	RCA	34.5	GFRP	120	50	25
	R-G-120-100	RCA	34.5	GFRP	120	100	50
C	N-G-180-0	NCA	32.2	GFRP	180	0	0
	N-G-180-50	NCA	32.2	GFRP	180	50	25
	N-G-180-100	NCA	32.2	GFRP	180	100	50
	R-G-180-0	RCA	34.5	GFRP	180	0	0
	R-G-180-50	RCA	34.5	GFRP	180	50	25
	R-G-180-100	RCA	34.5	GFRP	180	100	50
D	N-S-180-0	NCA	36.8	Steel	180	0	0
	N-S-180-50	NCA	36.8	Steel	180	50	25
	N-S-180-100	NCA	36.8	Steel	180	100	50
	R-S-180-0	RCA	38.2	Steel	180	0	0
	R-S-180-50	RCA	38.2	Steel	180	50	25
	R-S-180-100	RCA	38.2	Steel	180	100	50

Abbreviations: GFRP, glass fiber-reinforced polymer; NCA, natural coarse aggregates; RCA, recycled coarse aggregates.

geometric parameters and rebar arrangements. Each group's samples were axially loaded at three various eccentricity/width ratios, e/h = 0 (no eccentricity), e/h = 0.25 (moderate eccentricity, e = 50 mm), and e/h = 0.5 (high eccentricity, e = 100 mm). The dimensions of the samples were determined by the testing machine's capacity and a slenderness limit as specified by ACI 318-19ACI 318-19[37] and CSA A23.319CSA A23.319[38] for short columns, where, L_e and r signifies the effective length and the gyration radius of the cross-section, respectively.

3 | SPECIMENS' PREPARATION AND LOADING CONDITIONS

In this study, reinforcement cages were fixed into the wood molds with 25 mm spacing from the mold's walls

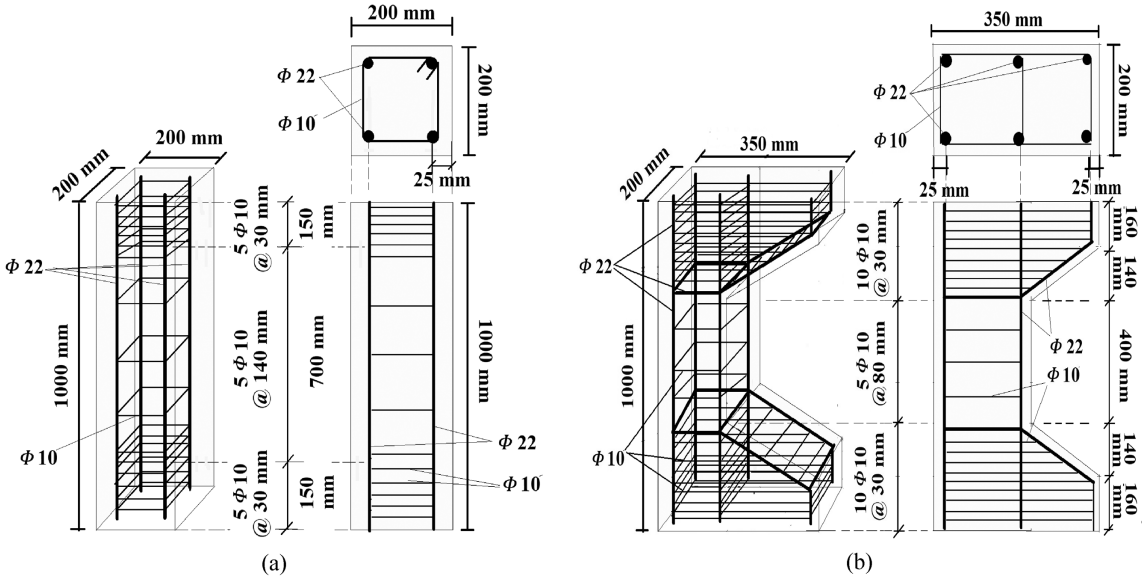

FIGURE 2 Geometry of columns and rebars arrangement under

FIGURE 3 Schematic photo of the columns' arrangement and test setup under. (a) Concentric load. (b) Eccentric load. LVDTs, linear variable displacement transducers

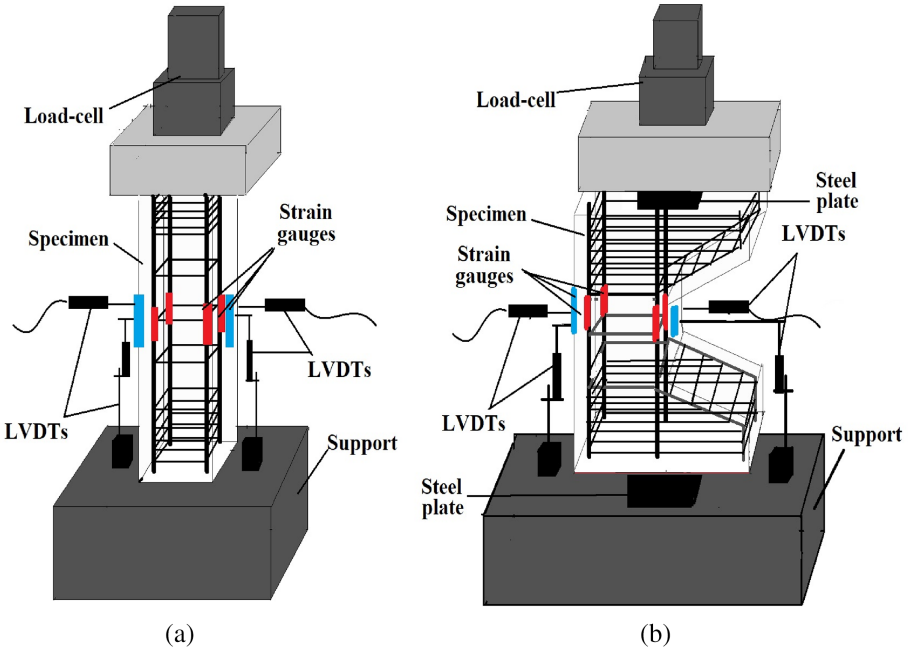

with the use of a spacer. Then, after mixing materials into a mixer, the fresh concrete was cast into the molds. Samples were removed from the molds after 24 h and entered the curing stage. During the curing phase, the samples were irrigated daily for 28 days. A cotton sack was used to maintain wet conditions. Also, in order to prevent water evaporation during the day, the samples were covered with thick nylon after irrigation. At 28 days of curing, the molds were opened and the samples were taken out and tested. Schematic and actual photos of specimens conducted under the concentric and eccentric loads are illustrated in Figures 3 and 4, respectively. Specimens were conducted under a hydraulic jack. To apply a load, a 5000 kN capacity load cell was used. The columns were confined at both ends with steel caps with a thickness of 5 mm and a total depth of 100 mm according to Xing et al.[39] The internal dimensions of the caps were equal to the dimension of the column which endorsed failure lengthways of the columns' length between the haunches. The test was done under displacement control conditions rate of 0.2 mm/min and the stopping condition was set to be the complete failure of columns. Electrical strain gauges were installed vertically on the concrete surface and on two of the longitudinal rebars at

(a) (b)

FIGURE 4 Actual photo of the columns' arrangement and test setup under. (a) Concentric load. (b) Eccentric load.

midheight on both the compression side and tension side of the columns. In addition, strain gauges were connected vertically on the surface of the concrete and the longitudinal reinforcement to assess the strain of concrete and both tensile and compressive longitudinal rebars. Additionally, two linear variable displacement transducers (LVDTs) were also installed at the midheight of the specimens to record the vertical and lateral displacements during the tests. The strain gauges and the LVDTs were connected to a data-gaining system that recorded five readings per second.

4 | RESULTS AND DISCUSSION

4.1 | Axial and flexural capacities of specimens

In this section, the axial and flexural capacities of samples are studied. The capability of specimens was normalized per compressive strength of concrete to consider the influence of the compressive strength, as below:

$$P_{\text{normalized}} = P_{\text{u}}/0.85f'_{\text{c}}A_{\text{g}} \quad (1)$$

In which, $P_{\text{normalized}}$, P_{u}, f'_{c}, and A_{g} denote the normalized axial resistance, the ultimate resistance of RC columns, the compressive strength of concrete, and the cross-section area of specimens, respectively. The obtained results of the load-bearing capacity of samples are presented in Table 8. Specimens' resistance was also tested under the simultaneous effect of axial load and flexural moment. Therefore, the normalized axial force and flexural bending were obtained using the following equations:

$$P_{\text{norm}} = P_{\text{u}}/f'_{\text{c}}A_{\text{g}} \quad (2)$$

$$M_{\text{norm}} = M_{\text{u}}/f'_{\text{c}}A_{\text{g}}h \quad (3)$$

where, P_{norm}, M_{norm}, M_{u}, and h indicate the maximum normalized axial load-bearing capacity and moment of the column, the maximum flexural moment, and the cross-section width (200 mm in this study). The maximum flexural moment includes two values: eccentricity and flexural capacity (M_{u1}) and the flexural moment due to lateral midheight deflections (M_{u2}). To calculate moments, the following formulas were utilized:

$$M_{\text{u1}} = P_{\text{u}}e \quad (4)$$

$$M_{\text{u2}} = P_{\text{u}}\Delta \quad (5)$$

In which, e and Δ denote the eccentricity distance and midheight lateral deflection at the maximum applied load, respectively. Previous investigations recommended that the load-moment interaction curve could be developed for RC columns reinforced by FRP rebars similar to those reinforced by steel bars.[40–42] While there is no recommendation in references ACI 318-19,[37] and CSA S6-19[43] about the load-moment interaction curve of FRP-reinforced columns. As a result, the nominal axial and flexural resistance of specimens were computed in two ways: discounting the influence of GFRP rebars in compression and considering it. For this aim, the following expectations were utilized to generate PM interaction illustrations for columns considering code limits from two design standards:

(1) The strain of concrete changes linearly according to the Euler-Bernoulli scheme; (2) the planer section continues plane after distortion, and the bond resistance between the concrete and rebars are constant; (3) the strain compatibility and forces equilibrium are fulfilled; (4) the rectangular stress block is used to calculate the compressive stress distribution over the compressive region of cross-section similar to that for steel RC columns[37,38]; (5) the maximum compressive strain of concrete is considered 0.0035 and 0.003[37,38]; (6) the tensile

TABLE 8 Summary of obtained outcomes

Group	Specimen	P_u (kN)	$P_{normalized}$ (kN)	$\varepsilon_{c1}(\mu\varepsilon)$	$\varepsilon_{c2}(\mu\varepsilon)$	$\varepsilon_{bar1}(\mu\varepsilon)$	$\varepsilon_{bar2}(\mu\varepsilon)$	δ (mm)	Δ(mm)	P_{bar}(kN)	$\frac{P_{bar}}{P_u}$ (%)
A	N-G-60-0	2009.3	1.56	−2612	—	−3934	—	1.04	—	375	18.6
	N-G-60-50	1378.2	1.07	−3316	490	−12,991	7768	1.2	1.23	—	—
	N-G-60-100	631.1	0.49	−2273	1254	−8792	6953	0.48	2.49	—	—
	R-G-60-0	2263.2	1.64	−2342	-	−3005	—	0.84	-	385	17.0
	R-G-60-50	1531.8	1.11	−2157	420	−3697	869	0.6	1.02	—	—
	R-G-60-100	690.0	0.50	−2103	985	−6722	5088	0.44	1.85	—	—
B	N-G-120-0	1790.3	1.39	−2911	—	−4950	—	1.4	—	246	13.7
	N-G-120-50	1223.6	0.95	−2594	520	−5850	2240	0.88	1.67	—	—
	N-G-120-100	605.4	0.47	−2545	1387	−4221	4639	0.72	2.82	—	—
	R-G-120-0	2042.4	1.48	−2617	—	−3633	—	1.12	-	268	13.2
	R-G-120-50	1311.0	0.95	−2229	503	−5248	1489	0.76	1.34	—	—
	R-G-120-100	634.8	0.46	−2248	1302	−2979	3875	0.6	2.19	—	—
C	N-G-180-0	1584.2	1.23	−2660	—	−7728	—	1.84	—	122	7.7
	N-G-180-50	1107.7	0.86	−2845	851	−9030	4920	1.08	1.83	—	—
	N-G-180-100	592.5	0.46	−2890	1892	−4108	2325	1	3.12	—	—
	R-G-180-0	1821.6	1.32	−2483	—	−6791	—	1.48	—	139	7.6
	R-G-180-50	1173.0	0.85	−2607	752	−4362	603	0.92	1.61	—	—
	R-G-180-100	634.8	0.46	−2621	1625	−3612	1450	0.8	2.98	—	—
D	N-S-180-0	1751.7	1.19	−3133	—	−8958	—	2.36	—	396	22.6
	N-S-180-50	1148.2	0.78	−2410	1156	−5180	848	0.72	2.04	—	—
	N-S-180-100	662.4	0.45	−3745	2014	−12,291	9549	1.48	3.49	—	—
	R-S-180-0	1971.1	1.29	−3042	—	−7844	—	2	—	405	20.5
	R-S-180-50	1268.2	0.83	−2920	958	−10,922	5878	0.84	1.92	—	—
	R-S-180-100	702.9	0.46	−3345	1865	−10,518	7513	1.2	3.72	—	—

resistance of concrete is ignored; (7) a linear-elastic performance is considered for the stress–strain relationship of GFRP rebars; (8) based on those explained above in the first state (ignoring GFRP bars influence), the axial capacity was determined using Equations (6) and (8), respectively[37,38]:

$$P_n = \alpha_1 f'_c \left(A_g - A_f\right) \tag{6}$$

$$\alpha_1 = 0.85 - 0.0015 f'_c \geq 0.67 \tag{7}$$

$$P_n = 0.85 f'_c \left(A_g - A_f\right) \tag{8}$$

(9) The axial strength was measured using Equations (9) and (10), considering the impact of GFRP (State 2):

$$P_n = \alpha_1 f'_c A_g + 0.0035 E_{ft} A_f \tag{9}$$

$$P_n = 0.85 f'_c A_g + 0.0035 E_{ft} A_f \tag{10}$$

State 1. in this state, Equations (11) and (12) were utilized to measure the compressive and bending strength for different eccentricity distances, respectively, as illustrated in Figure 5.

$$P_n = C_c - \varepsilon_f E_{ft} A_f \tag{11}$$

$$M_n = C_c y_c \pm \varepsilon_f E_{ft} A_f y_{ft} \tag{12}$$

where, C_c, y_c, and y_{ft} denote the compressive stress resultant of concrete, the distance between the center of the compressive region and the center of cross-section, and the distance between the center of tension rebars and the center of cross-section, respectively. Therefore,

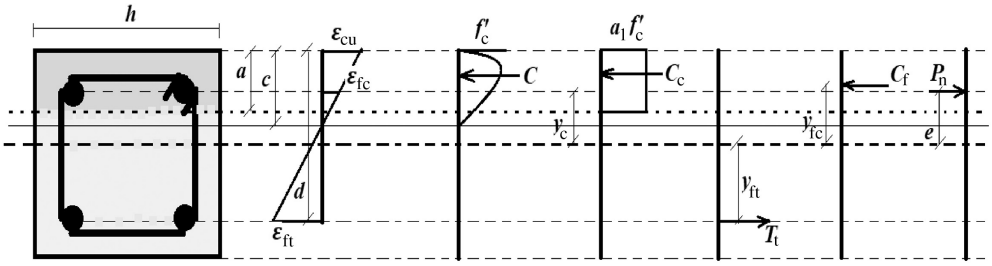

FIGURE 5 Stress distribution and forces equilibrium of columns

the compressive stress of concrete would be calculated as below:

$$C_c = \alpha_1 f'_c A_c \tag{13}$$

$$y_c = \frac{h}{2} - \frac{a}{2} \tag{14}$$

$$A_c = ab \tag{15}$$

$$a = \beta_1 c \tag{16}$$

$$\beta_1 = 0.97 - 0.0025 f'_c \geq 0.67 \tag{17}$$

$$\beta_1 = 0.85 - 0.05\frac{f'_c - 28}{7} \geq 0.65 \tag{18}$$

In which, A_c, c, a, and h indicate the cross-section area of the compressive region, the neutral axis depth, the rectangular stress block depth, and the cross-section width, respectively (Figure 5). In addition, the values of α_1 and β_1 was considered as per ACI 318-19[37] and CSA A23.3-19.[38]

State 2. In this state, the compression contribution of GFRP rebars was taken into account; however, similar formulas to State 1 were used with the following modifications.

$$P_n = C_c + \varepsilon_c E_{ft} A_f - \varepsilon_f E_{ft} A_f \tag{19}$$

$$M_n = C_c y_c \pm \varepsilon_c E_{ft} A_f y_{fc} \pm \varepsilon_f E_{ft} A_f y_{ft} \tag{20}$$

where, ε_c and y_{fc} are the strain of compressive GFRP rebars and the distance between the center of the cross-section and compressive rebars, respectively. Conversely, there is no model to determine the P-M behavior of FRP-reinforced columns in CSA S6-19,[43] ACI 440.1R-15,[44] and AASHTO,[45] and these standards neglected the impact of FRP reinforcements when employed as compression bars. CSA S6-19,[43] ACI 440.1R-15,[44] and AASHTO[45] proposed different requirements to measure the performance of FRP-reinforced beams, slabs, and other RC members except for columns. Additionally, CSA S806-12 (2017) allows GFRP rebars to be used to reinforce RC columns. When calculating the ultimate axial resistance of GFRP-RC columns, CSA S806-12 (2017) advises ignoring the effect of the GFRP longitudinal rebars. Therefore, the ultimate resistance of GFRP-RC columns can be estimated using the following formulas as per CSA S806-12 (2017):

$$P_{r0} = \alpha_1 \phi_c f'_c (A_g - A_f) \tag{21}$$

$$\alpha_1 = 0.85 - 0.0015 f'_c \geq 0.67 \tag{22}$$

where, $\phi_c = 0.85$. Additionally, CSA S806-12 (2017) restricts the ratio of the longitudinal bars to as same as those for steel reinforcement; min: 1% and max: 8%. Moreover, the ultimate flexural resistance of GFRP-RC columns was developed by previous studies based on CSA S806-12 (2017):

$$M_r = C_c\left(\frac{h}{2} - \frac{\beta_1 c}{2}\right) \pm \sum T_f(y_f) \tag{23}$$

$$C_c = \alpha_1 \phi_c f'_c \beta_1 cb \tag{24}$$

$$T_f = A_f \phi_f E_f \sum \varepsilon_f \tag{25}$$

$$\beta_1 = 0.97 - 0.0025 f'_c \geq 0.67 \tag{26}$$

$$\frac{c}{d} = \frac{0.0035}{0.0035 + \varepsilon_f} \tag{27}$$

where, E_f and ε_f indicate elastic modulus and strain of GFRP, respectively. The summary of obtained experimental results is listed in Table 8.

Furthermore, Figure 6 shows the comparison between the experimental results and models proposed by existing standards. Generally, the resistance of RC columns declined with an increase in the eccentricity distance due to increasing the flexural moment. While the

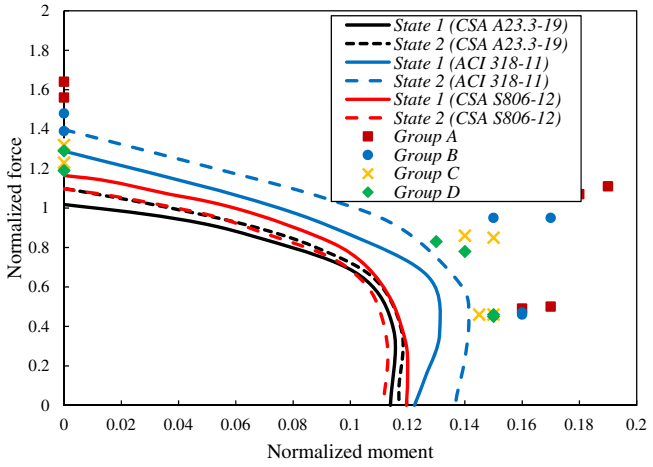

FIGURE 6 Comparison between the experimental and numerical results of load-bending interaction curve

incorporation of RCA led to improving the axial resistance of GFRP-RC columns. The improvement influence of used RCA could be associated with the higher strength of used aggregates in comparison to NCA as well as the higher broken surface of RCA. Conversely, the share of longitudinal GFRP rebar was decreased with an increase in the eccentricity distance due to swelling of the flexural condition on the reinforcements. As described above on the proposed models by standards, the obtained results were compared with the P–M interaction plans for the columns, as illustrated in Figure 6. There, the load-bearing capacity of RC columns was enhanced with a reduction in the stirrup spacing as well as using the RCA which could be associated with an increase in confinement when higher transverse rebars (lower spacing) was used. The obtained results showed a higher load-bearing capacity compared with the proposed P–M interaction diagram by ACI 318-19,[37] CSA A23.3-19,[38] and the developed model of CSA S806-12 (2017) under a concentric load. In addition, reducing the stirrup spacing significantly affected the compressive performance under the eccentric load. It was observed that using longitudinal GFRP rebars substantially affected the maximum load-bearing capacity of RC columns due to the higher strength of GFRP bars in comparison with steel. According to Figure 6, the obtained results of GFRP-reinforced specimens made by RCA were much higher than those recommended interaction diagrams by ACI 318-19,[37] CSA A23.3-19,[38] and the developed model of CSA S806-12 (2017). Besides, the proposed expectations with ACI 318-11 (2019) and CSA A23.3–19[38] and the developed model of CSA S806-12 (2017) for GFRP-RC specimens underestimate the load-bearing capacity under the eccentricity load by an average of 12% and 18% and 23% for 50 and 100 mm eccentricity distance load, respectively. This could be due to GFRP's higher tensile strength than steel rebars, which increased the resistance contribution of GFRP reinforcement on the tension side as the eccentricity distance was increased.

4.2 | Load–displacement relationship of specimens

Figure 7 shows the normalized axial load–displacement relationship of columns. Regarding this figure, the maximum load-bearing capacity of samples was slightly enhanced with an increase in RCA content, while the maximum deflection declined. The higher strength of utilized aggregates compared with NCA and the higher fractured surface of RCA may both contribute to the improving influence of RCA on the strength of columns. Because the higher fractured surface of RCA in comparison to NCA results in increasing the adhesion between aggregates and concrete paste and improved resistance of RC columns. Furthermore, the bond performance of GFRP rebars in RCA concrete could be another essential factor in increasing the load-bearing capacity of columns. In this regard, Godat et al.[46] measured the bond strength of FRP rebars in RCA concrete. They showed that using RCA led to increasing the contact resistance and friction between FRP rebars and concrete. When RCA was utilized, there was also an increase in bond resistance and a shift in failure mode from pull-out to concrete splitting. The use of FRP rebars in RCA concrete led to a postpeak slip hardening performance, according to their findings, which leads to improving the axial behavior of RC columns. This was owing to the rebar's friction resistance, which was mainly attributable to the FRP reinforcement surface treatment and the RCA's coarser surface. Conversely, reducing transverse reinforcement spacing led to increasing the maximum axial strength and reducing the bending of RC columns. Besides, the impact of RCA on the axial resistance of specimens was decreased by reducing the stirrup spacing, which shows the reducing the contribution results of RCA on improving the axial performance of RC columns.

Furthermore, the maximum axial strength and displacement were considerably decreased when specimens were conducted under an eccentric load, and the axial performance of columns was further decreased when the eccentricity distance increased (Figure 7b,c). In addition, the initial slope of load–displacement curves was amplified by reducing the stirrup spacing or using RCA, which shows the improvement in the stiffness of RC columns. As a result, for specimens tested under the concentric load, using RCA improved the final resistance. However, in columns subjected to the eccentric load, the influence

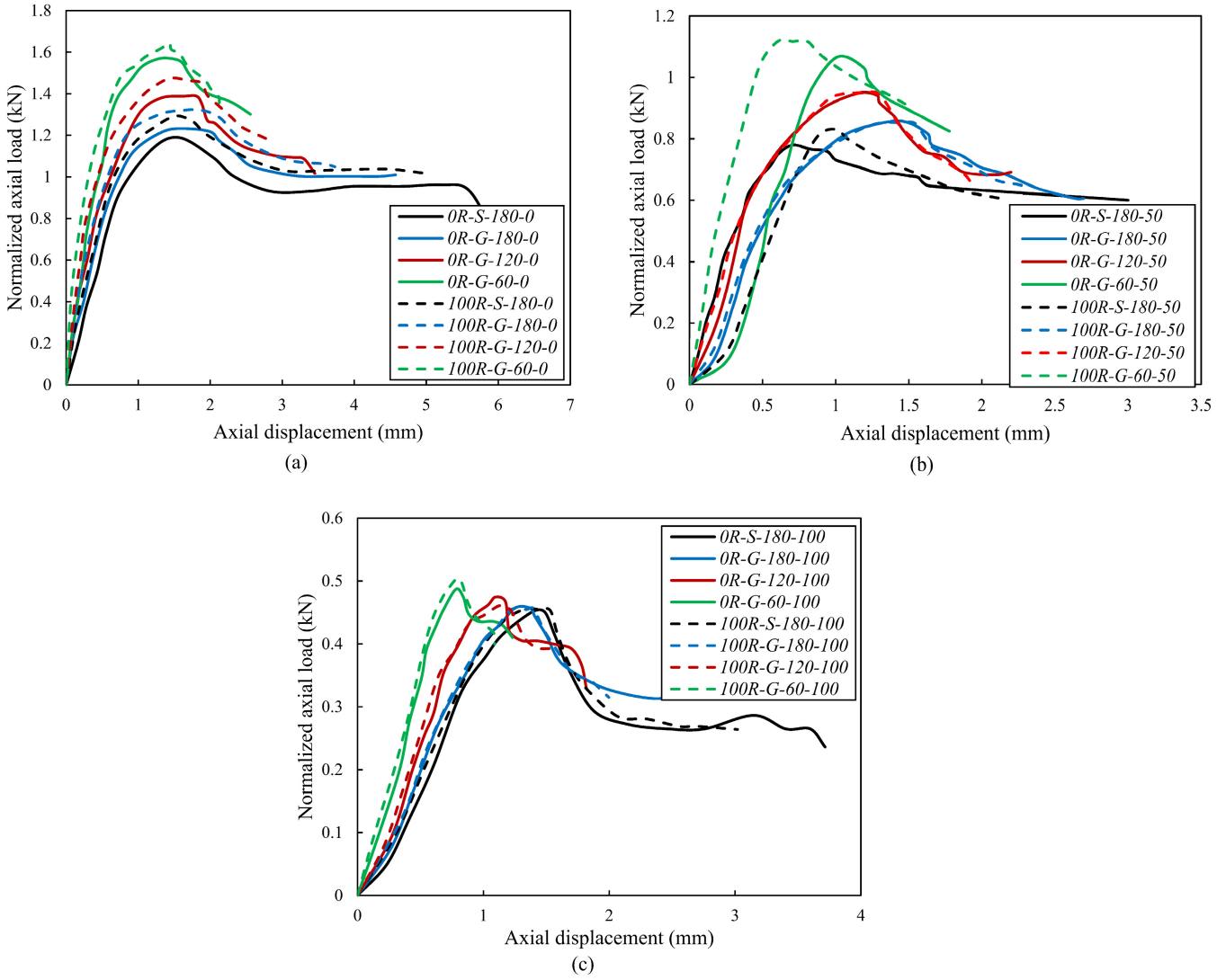

FIGURE 7 Normalized load-axial deformation of specimens under (a) concentric load, (b) 50 mm eccentric load, and (c) 100 mm eccentric load

of RCA on increasing the stiffness of RC columns was significant. In addition, in specimens tested under a concentric load, using RCA improved the axial performance of GFRP-RC columns by about 25% and 35% when the stirrup spacing decreased by 60 and 120 mm, respectively. While the maximum displacement declined by 53% and 67% when 100% RCA was used, and the stirrup spacing decreased by 60 and 120 mm, respectively.

4.3 | Modes of failure

Figure 8 provides a mode of failure of typical specimens. These results showed that the incorporation of RCA led to reducing the cracks width with more propagation at the midheight of specimens. In addition, utilizing GFRP longitudinal rebars caused a reduction in the cracks width due to improving the bond-slip resistance between the concrete and GFRP compared with that of steel rebars. Therefore, the minimum crack width was observed when both RCA and GFRP reinforcements were used simultaneously. Thus, more cracks were concentrated at the midheight of columns with an increase in the stirrup spacing, and the crack width was increased meaningfully as well. As a result of increasing the load value, vertical and horizontal fractures line occurred at the midheight of RC columns and then propagated to the two ends and edges of the specimens. Conversely, specimens conducted under the concentric load failed in compressive modes by cracking the concrete cover without buckling. For those specimens subjected to an eccentric load, vertical and inclined cracks were observed at the

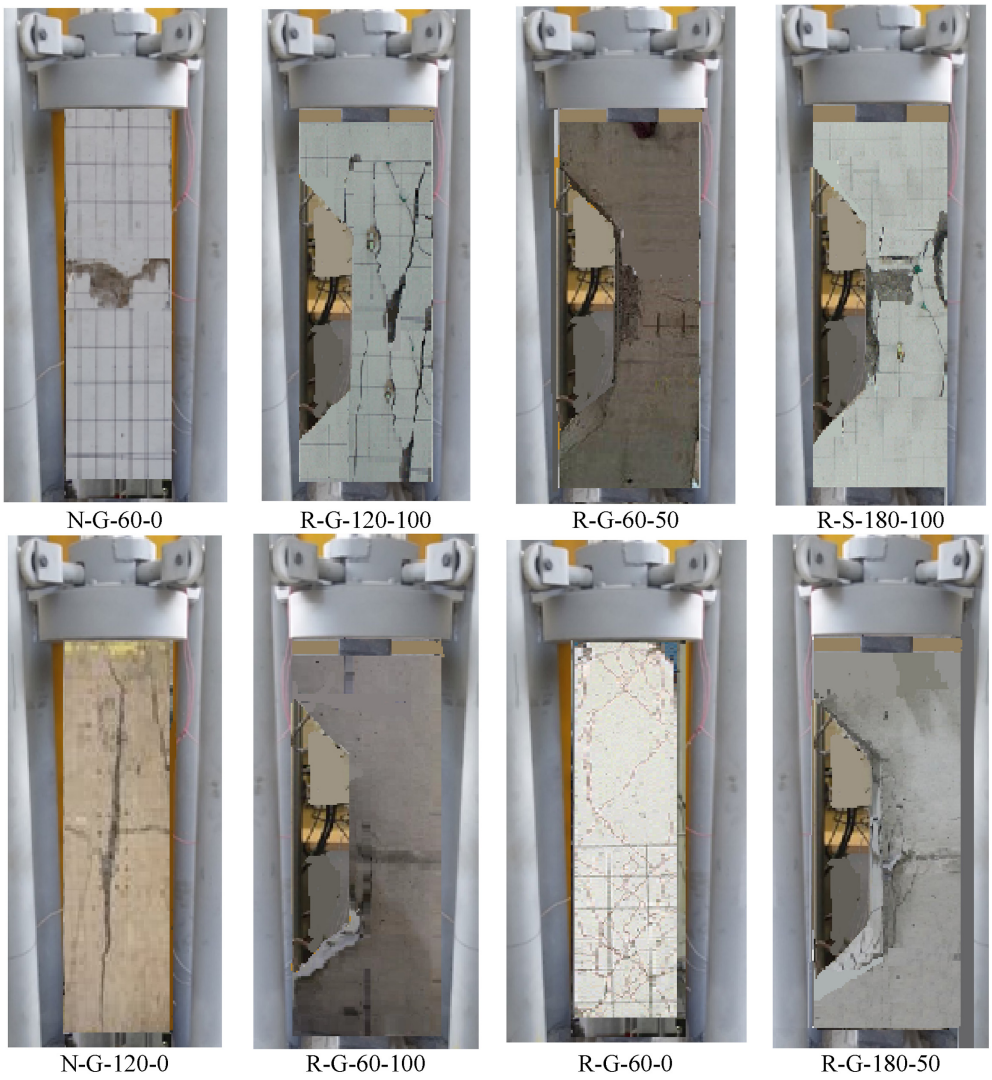

FIGURE 8 Mode of failure of typical specimens

midheight of specimens propagated by horizontal cracking in the tension region of columns. Besides, by increasing the load, the inclined crakes are more propagated. While the incorporation of RCA led to reducing the inclined cracks width as provided in Table 9.

Regarding Table 9, the ultimate crack width of GFRP-RC columns under a concentric load decreased respectively by 42%, 52%, and 77% when RCA was used and 180 mm, 120 mm, and 60 mm transverse reinforcement spacing was provided, relative to the similar specimens reinforced by steel rebars. Conversely, increasing the eccentricity distance resulted in increasing the maximum crack width while the incorporation of RCA restricted the increase in crack width. Therefore, for GFRP-RC columns subjected to a 100 mm eccentricity distance load and confined by 180 mm, 120 mm, and 60 mm stirrup spacing, using 100% RCA decreased the maximum cracks width by 33%, 52%, and 74%, respectively, compared with the similar steel-reinforced concrete columns made with NCA.

4.4 | Ductility

In this section, the ductility of columns was assessed, and the influence of RCA, stirrup spacing, and eccentricity length on the ductility of specimens was studied. A more appropriate concept of a ductility ratio was defined by Pessiki and Pieroni.[47] According to their definition, this index is the ratio of the displacement at 85% of the maximum load on the postpeak portion of the curve (Δ_u) to the displacement at the initial yield of the column (Δ_y) (Equation 28), as shown in Figure 9. The obtained results of the specimens' ductility are presented in Figure 10. Increasing the ductility ratio denotes deform failure; however, specimens fail suddenly when the ductility ratio decreases.

$$i = \Delta_u / \Delta_y \tag{28}$$

According to Figure 10, the ductility of RC columns was improved with a decrease in the transverse rebar

TABLE 9 Summary of cracking and failure in specimens

Group	Specimen	Cracking load (kN)	Failure load (kN)	Maximum crack width (mm)
A	N-G-60-0	10.0	2009.3	12
	N-G-60-50	6.8	1378.2	16
	N-G-60-100	3.2	631.1	19
	R-G-60-0	11.6	2263.2	8
	R-G-60-50	7.7	1531.8	11
	R-G-60-100	3.4	690.0	12
B	N-G-120-0	7.2	1790.3	17
	N-G-120-50	4.8	1223.6	21
	N-G-120-100	2.4	605.4	27
	R-G-120-0	8.2	2042.4	14
	R-G-120-50	5.2	1311.0	18
	R-G-120-100	2.5	634.8	22
C	N-G-180-0	4.7	1584.2	26
	N-G-180-50	3.3	1107.7	32
	N-G-180-100	1.8	592.5	38
	R-G-180-0	5.5	1821.6	20
	R-G-180-50	3.5	1173.0	30
	R-G-180-100	1.9	634.8	31
D	N-S-180-0	5.3	1751.7	35
	N-S-180-50	3.4	1148.2	42
	N-S-180-100	1.9	662.4	46
	R-S-180-0	5.9	1971.1	29
	R-S-180-50	3.8	1268.2	36
	R-S-180-100	2.1	702.9	39

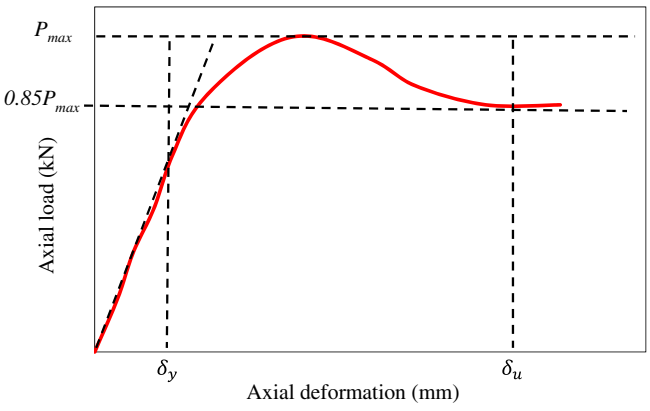

FIGURE 9 Definition of ductility ratio

spacing. In addition, the use of RCA instead of NCA led to a slight improvement in ductility. Therefore, reducing the transverse rebar spacing as well as the RCA incorporation prevents a sudden failure in RC columns. Thus, the maximum ductility could be obtained when RCA was used, and transverse reinforcement spacing was declined, as well. The results exhibited that the incorporation of RCA improved the ductility of RC columns under the concentric load by about 125%, 85%, and 30% when GFRP longitudinal rebar was used and 60, 120, and 180 mm stirrup spacing was provided, respectively, relative to that control steel-RC column with 180 mm transverse reinforcement spacing. Conversely, in those columns conducted under an eccentric load with 100 mm eccentricity distance, using RCA enhanced the ductility by 75%, 58%, and 15% when GFRP longitudinal rebar was used, and 60, 120, and 180 mm stirrup spacing were provided, respectively, compared with those of the control samples.

4.5 | Strain of rebars and concrete

The axial load versus the strain of concrete and longitudinal rebars was studied, as illustrated in Figures 11 and 12. Regarding the results, the initial slopes were

FIGURE 10 Influence of different variables on the ductility of RC columns

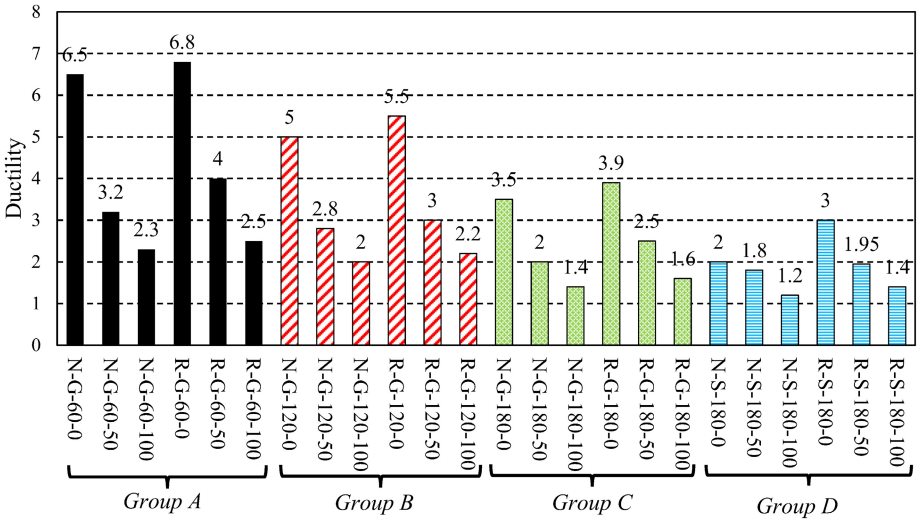

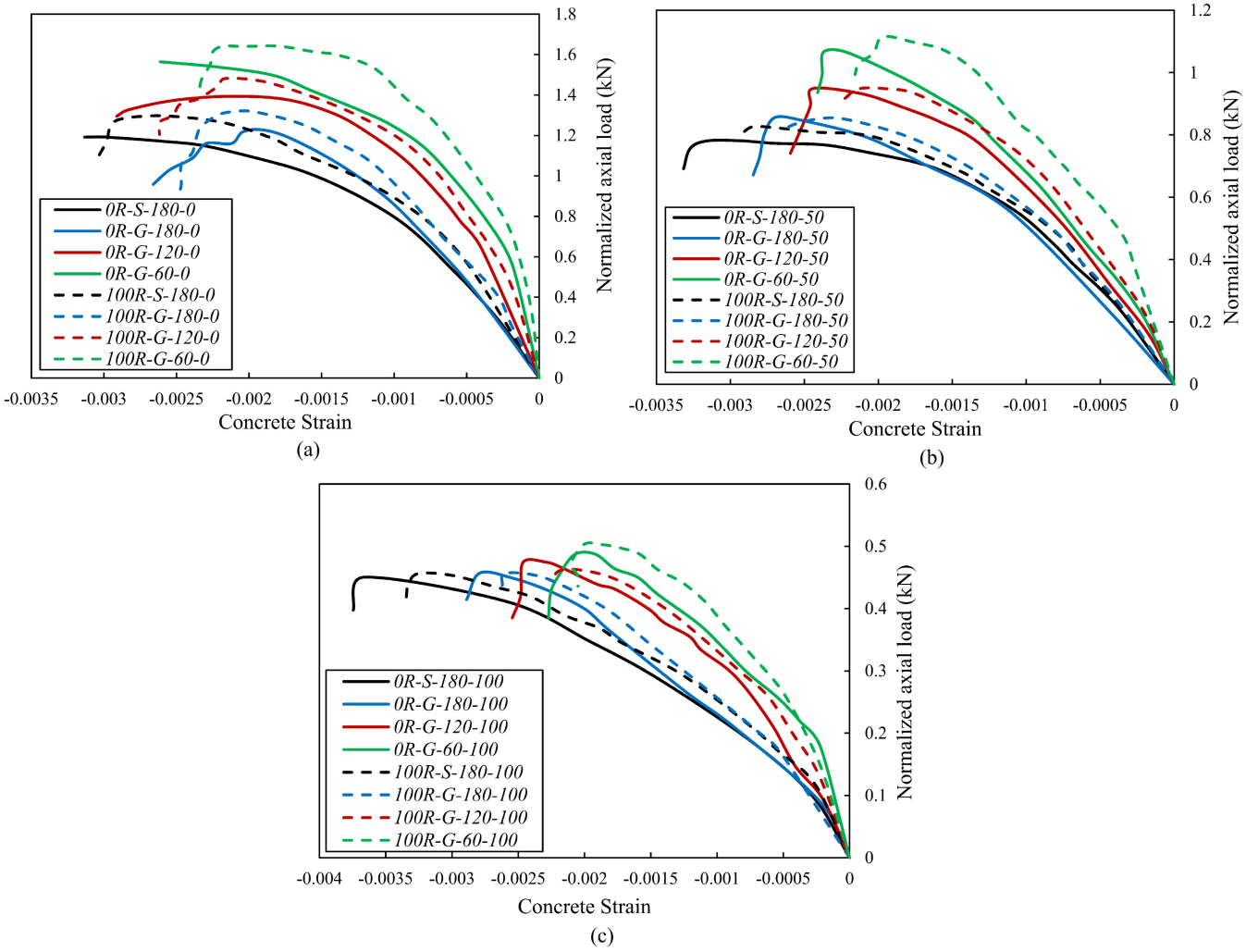

FIGURE 11 Axial load-concrete strain relationship of specimens under (a) concentric load, (b) 50 mm eccentricity, and (c) 100 mm eccentricity

significantly influenced by increasing the eccentricity distance, and the slope increased with a reduction in the eccentricity length. The concrete reaction was linear until fractures appeared, following which a nonlinear outflow developed until the maximum loads were reached. Concrete crushing was the most common mechanism of

failure for the tested columns, as evidenced by recorded concrete stresses at peak load. The compression and tension bars' axial strain responses are classified by an initial linear branch that increases steadily until micro cracks begin to happen. Hence, the maximum strain of concrete for specimens produced by NCA and RCA under the concentric load was 0.0033–0.0027 and 0.0029–0.0023, respectively. Therefore, the incorporation of RCA led to reducing the strain of concrete. This could be associated with the higher bond-slip resistance of RCA and rebars, which is attributable to the higher fractured surface of RCA compared with NCA. The same reduction influence on the strain of longitudinal rebars was observed because of using RCA. Liu et al.[48] showed that a reduction in the strain of FRP occurred with an increase in RCA contents. In addition, the strain of concrete was considerably decreased with the use of GFRP rebars as a longitudinal reinforcement because GFRP reinforcement has a higher yield strength than steel rebars. Furthermore, reducing transverse reinforcement spacing as well as using RCA led to increasing the normalized load versus the strain of concrete or longitudinal reinforcement. Therefore, in tested specimens under a concentric load, the strain of concrete decreased by 26%, 28%, and 33% when both RCA and GFRP were used, and transverse reinforcement spacing was 180, 120, and 60, respectively, relative to those steel-RC columns.

Additionally, in specimens subjected to an eccentric load with a 100 mm eccentricity length, the incorporation of RCA decreased the concrete strain of GFRP-RC columns by 28%, 42%, and 45% when 180, 120, and 60 mm stirrup spacing was provided, respectively. Under 50 mm and 100 mm transverse reinforcement spacings, the longitudinal rebars were conducted under both compressive and tensile stresses, although the value of compressive stress was much lower than that of tensile stress (Figure 12). As shown in Figure 12, reducing the stirrup

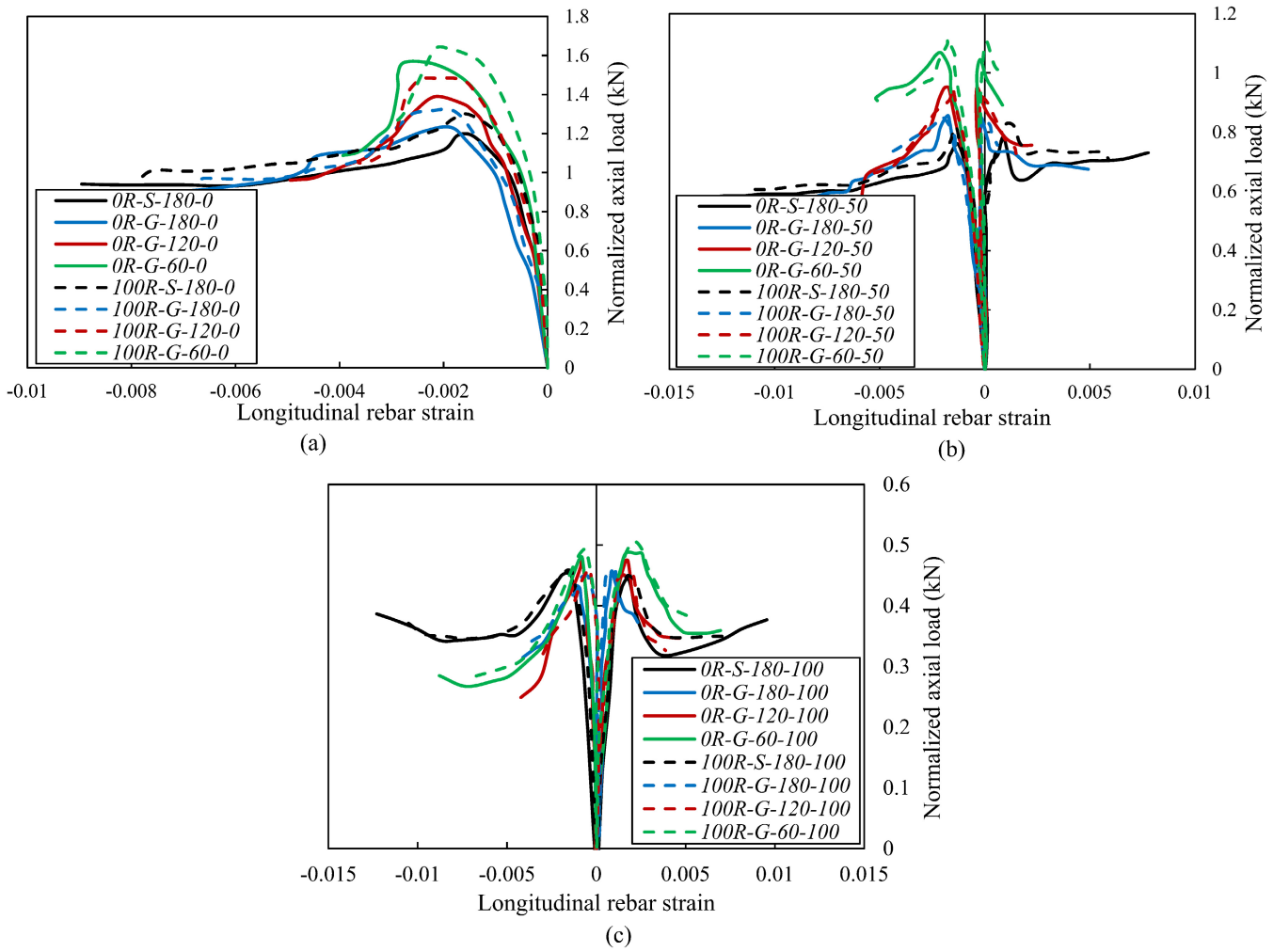

FIGURE 12 Axial load-longitudinal rebar strain relationship of specimens under (a) concentric load, (b) 50 mm eccentricity, and (c) 100 mm eccentricity

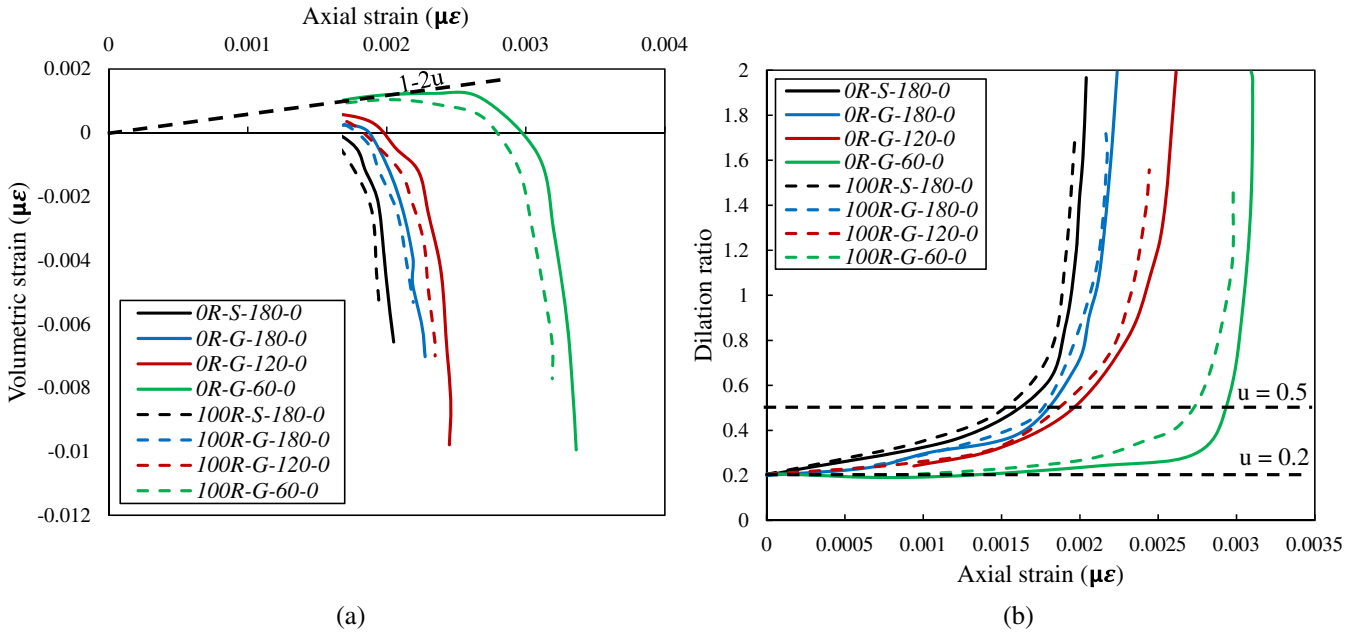

FIGURE 13 Confinement influence on the (a) volumetric stain and (b) dilation strain

spacing led to reducing the share of longitudinal rebar participation so that the strain of longitudinal rebars was considerably decreased. It was also found that using RCA played a vital role in reducing the strain of longitudinal rebars due to increasing the adhesive between longitudinal rebar and RCA compared with those of NCA. While, by increasing the eccentricity length, the influence of RCA on the maximum load and strain of longitudinal rebars decreased, which shows reducing the share of RCA participation.

4.6 | Confinement efficiency

The effect of stirrup on the prepeaks and postpeaks cracking characteristics of columns under a concentric load was assessed using the volumetric stress–strain response, ε_v, which is demarcated as the change in volume per unit volume in a triaxial condition of stress and may be calculated as:

$$\varepsilon_v = \varepsilon_a + 2\varepsilon_l \tag{29}$$

Where, ε_v, ε_a, and ε_l denote the volumetric, axial, and lateral strain, respectively. The obtained results are illustrated in Figure 13. A positive volumetric strain is thought to suggest volume drop, while a negative fraction indicates volume increase (Figure 13a). Furthermore, the dilation fraction, defined as the ratio of adjacent to axial strain, was employed to assess the transverse reinforcement's confinement efficiency (Figure 13b). When the concrete axial strain reaches ranges between 0.0018 and 0.003 for samples strengthened by stirrup spacing from 180 to 60 mm at the uneven crushing phase, this ratio approaches 0.5, beyond which it climbs with an almost vertical slope. The use of GFRP as longitudinal rebars also resulted in a slight increase in axial strain versus the dilation ratio. However, the axial strain decreases insignificantly when the RCA was incorporated. Alternatively, when the axial strain reached 0.0018, the dilation ratio increased with a virtually vertical slope. Regarding Figure 13a, the early slope of all specimens is adjacent to 1–2 υ, where, υ indicated the Poisson's ratio of the plain concrete $(\upsilon = 0.2)$, which agreed with the elastic state. A similar result could be found in Figure 13b. Regarding this figure, the postpeak behavior of samples with the stirrup spacing of 180 and 120 mm increased progressively in the same way, exhibiting stable crack propagation.

5 | CONCLUSION

This study aims to measure the axial performance of GFRP-reinforced concrete columns containing RCA under concentric and eccentric loading conditions. A total of 24 samples were reinforced and strengthened with longitudinal steel, and GFRP rebars and the load–displacement behavior, strain, and ductility of specimens were studied. RCA was used at two contents of 0% and 100% in terms of weight. Additionally, the influence of the stirrup was considered by providing three different spacings: 60, 120, and 180 mm. Specimens were conducted under various eccentricity ratios (e/h):

0 (no eccentricity), 0.25 (moderate eccentricity), and e/h = 0.5 (high eccentricity). Therefore, the following conclusion can be formed based on the findings:

1. The axial resistance of RC columns was improved with the use of GFRP as longitudinal rebars, and their strength was further enhanced when RCA was also used. While the share of longitudinal GFRP rebar loading and the effect of RCA declined with an increase in the eccentricity distance.
2. The requirements of standards underestimated the load-bearing capacity of RC columns under the eccentricity load when RCA was used, stirrup spacing was also decreased, and the predicted axial strength of columns reinforced by GFRP and produced by RCA were much higher than those P–M interaction diagrams that recommended standards.
3. Cracks width declined and crack more propagated with the use of RCA. Using longitudinal GFRP rebars led to reducing the cracks width, and the minimum crack width occurred when both RCA and longitudinal GFRP rebars were used together.
4. The ductility of GFRP-RC columns was improved with a reduction in the stirrup spacing. The incorporation of RCA led to a significant improvement in ductility. Therefore, reducing the transverse rebar spacing as well as the RCA incorporation prevents a sudden failure in RC columns.
5. The incorporation of RCA led to reducing the strain of concrete. Besides, the strain of concrete significantly decreased with the use of GFRP rebars. Reducing stirrup spacing as well as using RCA led to increasing the normalized load versus the strain of concrete and longitudinal reinforcement. While, by increasing the eccentricity distance, the influence of RCA on the maximum strain of longitudinal rebars decreased.

Finally, the results, presented in this study, are limited to specific dimensions for columns and materials characteristics for concrete. So, for future studies, it is recommended to consider a wide range of variables such as compressive strength of concrete, dimensions of columns, slenderness etc. The presented results of this study could also be utilized for comparison.

CONFLICT OF INTEREST

On behalf of all the authors, the corresponding author states that there is no conflict of interest.

DATA AVAILABILITY STATEMENT

The data that support the findings of this study are available from the corresponding author upon reasonable request.

ORCID

Arash Karimi Pour https://orcid.org/0000-0002-8456-4182
Amir Shirkhani https://orcid.org/0000-0003-2532-2906
Ehsan Noroozinejad Farsangi https://orcid.org/0000-0002-2790-526X

REFERENCES

1. Hadhood A, Mohamed HM, Benmokrane B. Experimental study of circular high-strength concrete columns reinforced with GFRP bars and spirals under concentric and eccentric loading. J Compos Construct. 2017;21(2):04016078.
2. Hadhood A, Mohamed HM, Benmokrane B. Assessing stress-block parameters in designing circular high-strength concrete members reinforced with FRP bars. J Struct Eng. 2018;144(10):04018182.
3. Sdiri A, Kammoun S, Daoud A. Numerical modeling of the interaction between reinforcement and concrete at early age—a comparison between glass fiber reinforced polymer and steel rebars. Struct Concr. 2020;22:1.
4. Experimental Investigations on Strengthened Reinforced Concrete Columns under Monotonic Axial Loading. (2021). International Journal of Engineering, 34(5). https://doi.org/10.5829/ije.2021.34.05b.06
5. Abdelazim W, Mohamed H, Afifi M, Benmokrane B. Proposed slenderness limit for GFRP-RC columns based on experiments and buckling analysis. ACI Struct J. 2020;117(1).
6. Garhwal S, Sharma S, Sharma SK. Monitoring the flexural performance of GFRP repaired corroded reinforced concrete beams using passive acoustic emission technique. Struct Concr. 2020;22:1.
7. Li S, Chan TM, Young B. Behavior of GFRP-concrete double tube composite columns. Thin-Walled Struct. 2022;178:109490.
8. Lu C, Cai Q, Xu K, Sha Z, Yan Y. Comparison of flexural behaviors between plain and steel-fibre-reinforced concrete beams with hybrid GFRP and steel bars. Structure. 2022;43:1–11.
9. Raza A, El Ouni MH, Ali L, Awais M, Ali B, Ahmad Z, et al. Structural evaluation of recycled aggregate concrete circular columns having FRP rebars and synthetic fibers. Eng Struct. 2022;250:113392.
10. Wu C, Hwang HJ, Ma G. Effect of stirrups on the bond behavior of lap spliced GFRP bars in concrete beams. Eng Struct. 2022;266:114552.
11. Xue W, Peng F, Fang Z. Behavior and design of slender rectangular concrete columns longitudinally reinforced with fiber-reinforced polymer bars. ACI Struct J. 2018;115(2):311–22.
12. De Luca A, Nanni A. FRP-reinforced concrete structures. In: Nicolais L, Borzacchiello A, Lee SM, editors. Wiley Encyclopedia of Composites. Hoboken, NJ: John Wiley & Sons; 2012.
13. Guérin M, Mohamed HM, Benmokrane B, Shield CK, Nanni A. Effect of glass fiber-reinforced polymer reinforcement ratio on axial-flexural strength of reinforced concrete columns. ACI Struct J. 2018;115(4):1049–3.
14. Hadhood A, Mohamed HM, Benmokrane B, Nanni A, Shield CK. Assessment of design guidelines of concrete columns reinforced with glass fiber-reinforced polymer bars. ACI Struct J. 2019;116(4):193–207.

15. Abdelazim W, Mohamed HM, Benmokrane B, Afifi MZ. Effect of critical test parameters on the behavior of glass fiber-reinforced polymer-reinforced concrete slender columns under eccentric load. ACI Struct J. 2020b;117(4):127–41.
16. Khorramian K, Sadeghian P. Experimental investigation of short and slender rectangular concrete columns reinforced with GFRP bars under eccentric axial loads. J Compos Construct. 2020;24(6):04020072.
17. Chellapandian M, Prakash SS, Sharma A. Experimental investigations on hybrid strengthening of short reinforced concrete column elements under eccentric compression. Struct Concr. 2019;20:6–1973.
18. Anvari A, Ghalehnovi M, De Brito J, Karimipour A. Improved bending behaviour of steel-fibre-reinforced recycled aggregate concrete beams with a concrete jacket. Mag Concr Res. 2021; 73(12):608–26.
19. Chaboki H, Ghalehnovi M, Karimipour A. Study of the flexural behaviour of recycled aggregate concrete beams. Concr Res. 2019;12(3):45–60.
20. Ghalehnovi M, Karimipour A, Anvari A, de Brito J. Flexural strength enhancement of recycled aggregate concrete beams with steel fibre-reinforced concrete jacket. Eng Struct. 2021; 240:112325.
21. Ghalehnovi M, Karimipour A, De Brito J, Chaboki HR. Crack width and propagation in recycled coarse aggregate concrete beams reinforced with steel fibres. Appl Sci. 2020; 10(21):7587.
22. Karimipour A. Effect of untreated coal waste as fine and coarse aggregates replacement eon the properties of steel and polypropylene fibres reinforced concrete. Mech Mater. 2020;150: 103592.
23. Karimipour A. Experimental and numerical evaluation of steel fibres RC patterns influence on the seismic behaviour of the exterior concrete beam-column connections. Eng Struct. 2022; 263:114358.
24. Breccolotti M, Materazzi AL. Structural reliability of eccentrically-loaded sections in RC columns made of recycled aggregate concrete. Eng Struct. 2010;32(11):3704–12.
25. Choi W-C, Yun H-D. Compressive behavior of reinforced concrete columns with recycled aggregate under uniaxial loading. Eng Struct. 2012;41:285–93.
26. Xu J-J, Chen Z-P, Ozbakkaloglu T, Zhao X-Y, Demartino C. A critical assessment of the compressive behavior of reinforced recycled aggregate concrete columns. Eng Struct. 2018;161: 161–75.
27. Sunayana S, Barai SV. Performance of fly ash incorporated recycled aggregates concrete column under axial compression: experimental and numerical study. Eng Struct. 2019;196:109258.
28. Tang Y, Fang S, Chen J, Ma L, Li L, Wu X. Axial compression behavior of recycled-aggregate-concrete-filled GFRP–steel composite tube columns. Eng Struct. 2020;216:110676.
29. Chen W, Yang H. Fracture performance of concrete incorporating different levels of recycled coarse aggregate. Struct Concr. 2020;22:1.
30. Shaikh FUA. Mechanical properties of concrete containing recycled coarse aggregate at and after exposure to elevated temperatures. Struct Concr. 2017;19:2.
31. ASTM C293-08. Standard test method for compressive strength of concrete (using simple beam with centre-point loading). Pennsylvania, United States: ASTM International; 2008.
32. BS EN 12390-2. Testing hardened concrete: making and curing specimens for strength tests. London, UK: British Standards Institution; 2000.
33. BS EN 12390-3. Testing hardened concrete: compressive strength of test specimens 19. London, UK: British Standards Institution; 2009.
34. BS EN. Testing hardened concrete: shape, dimensions and other requirements for specimens and moulds. Vol 12390-1. London, UK: British Standards Institution; 2000.
35. ASTM D7957/D7957M. Standard specification for solid round glass fiber reinforced polymer bars for concrete reinforcement. West Conshohocken, PA: ASTM International; 2017.
36. ASTM A615/A615M. Standard specifi11 for deformed and plain carbon-steel bars for concrete reinforcement. West Conshohocken, PA: ASTM International; 2020.
37. ACI 318-19. Building code requirements for structural concrete and commentary. Farmington Hills, MI: American Concrete Institute; 2019.
38. CSA A23.3-19. Design of concrete structures. Mississauga, Ontario: Canadian Standard Association; 2019.
39. Xing L, Lin G, Chen JF. Behavior of FRP-confined circular RC columns under eccentric compression. J Compos Constr. 2019; 24(4):04020030.
40. Afifi MZ, Mohamed HM, Chaallal O, Benmokrane B. Confinement model for concrete columns internally confined with carbon FRP spirals and hoops. J Struct Eng. 2015; 141(9):04014219.
41. Fan X, Zhang M. Behaviour of inorganic polymer concrete columns reinforced with basalt FRP bars under eccentric compression: an experimental study. Compos Part B Eng. 2016;104: 44–56.
42. Tobbi H, Farghaly AS, Benmokrane B. Behavior of concentrically loaded fiber-reinforced polymer reinforced concrete columns with varying reinforcement types and ratios. ACI Struct J. 2014;111(2).
43. CSA S6-19. Canadian highway bridge design code. Mississauga, Ontario: Canadian Standard Association; 2019.
44. ACI 440.1R-15. Design and construction of structural concrete reinforced with fiber-reinforced polymer bars. Farmington Hills, MI: American Concrete Institute; 2015.
45. AASHTO. A policy on geometric design of highways and streets. North Capitol Street, NW: American Association of State Highway and Transportation Officials; 2018.
46. Godat A, Aldaweela S, Aljaberi H, Al Tamimi N, Alghafri E. Bond strength of FRP bars in recycled-aggregate concrete. Construct Build Mater. 2021;267:120919.
47. Pessiki S, Pieroni A. Axial load behavior of LargeScale spirally reinforced HighStrength concrete columns. Struct J. 1997;94(3): 304–14.
48. Liu H, Yang J, Wang X. Bond behavior between BFRP bar and recycled aggregate concrete reinforced with basalt fiber. Construct Build Mater. 2017;135:477–83.

AUTHOR BIOGRAPHIES

Arash Karimi Pour
Department of Civil Engineering, University of Texas at El Paso (UTEP), USA
akarimipour@miners.utep.edu

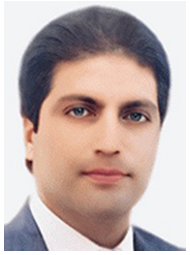

Amir Shirkhani
Department of Structural Engineering, Faculty of Civil Engineering, University of Tabriz, Tabriz, Iran
shirkhani@tabrizu.ac.ir

Mehmet Serkan Kırgız
Department of Architecture, Faculty of Engineering and Natural Sciences, İstanbul Sabahattin Zaim University, İstanbul 34303, Turkey
nakres42@yahoo.com

Ehsan Noroozinejad Farsangi
Department of Civil Engineering, The University of British Columbia (UBC), Vancouver, Vanada
ehsan.noroozinejad@ubc.ca

How to cite this article: Karimi Pour A, Shirkhani A, Kırgız MS, Noroozinejad Farsangi E. Experimental investigation of GFRP-reinforced concrete columns made with waste aggregates under concentric and eccentric loads. Structural Concrete. 2023;24(1):1670–88. https://doi.org/10.1002/suco.202200624